



1 **Forecasting coastal dune mobility: A logistic regression**
2 **model driven by meteorological data and climate indices**

3

4 Mauricio Toffani¹, Silvio Casadío²

5 ¹Instituto de Investigación en Paleobiología y Geología, UNRN – CONICET, General Roca, 8332,
6 Argentina

7 ² Universidad Andres Bello, Facultad de Ingeniería, Geología, Autopista Talcahuano, 7100 Concepción,
8 Chile

9 *Correspondence to:* Mauricio Toffani (mtoffani@unrn.edu.ar)

10



11 **Abstract**

12 Predicting dune mobility under changing climatic conditions remains a challenge in aeolian
13 geomorphology, particularly in data-scarce regions. This study presents a novel application of binomial
14 logistic regression to forecast dune activation and migration using readily available meteorological data.
15 We combine established dune mobility indices (Tsoar and Lancaster) into a new integrated index (TsoLa)
16 and evaluate its performance against observed dune migration rates derived from satellite imagery. The
17 model incorporates wind speed, precipitation, and the Southern Annular Mode (SAM) as predictors,
18 achieving robust predictive accuracy ($AUC > 0.75$) for two distinct coastal dune fields in NE Patagonia,
19 Argentina. Our results demonstrate that even with standard climatic inputs, logistic regression can
20 effectively identify periods of dune activity, offering a low-cost tool for coastal management. The approach
21 is transferable to other aeolian systems, providing a framework for assessing dune dynamics under current
22 and future climate scenarios.

23 **1. Introduction**

24 Predicting the mobility of coastal dunes in response to climatic variability remains a significant
25 challenge in aeolian geomorphology (Hugenholtz and Wolfe, 2005; Levin et al., 2014). Dune systems are
26 dynamic landscapes that reflect complex interactions between wind energy, sediment supply, vegetation
27 cover, and climatic oscillations (Hesp and Thom, 1990; Tsoar and Blumberg, 2002; Marcomini and
28 Maidana, 2006; Yizhaq et al., 2007, 2013; Miot da Silva and Hesp 2013; Miot da Silva et al., 2013; Hoover
29 et al., 2018; Louassa et al., 2018; Gao et al., 2023; Ren et al., 2024). While traditional approaches, such as
30 drift potential calculations and mobility indices, provide valuable descriptors of wind-driven sediment
31 transport (Fryberger and Dean, 1979; Lancaster, 1988; Tsoar, 2005), they offer limited predictive capacity
32 for forecasting dune activation or stabilization over time. This methodological gap is particularly relevant
33 in the context of climate change, where shifts in wind regimes, precipitation patterns, and storm frequency
34 may alter dune behavior with consequences for coastal ecosystems and human infrastructure (Jackson et
35 al., 2019a; Hesp et al., 2022).

36 Statistical modeling presents a promising pathway to bridge this gap. Binomial logistic regression
37 is well-suited for predicting binary geomorphic outcomes—such as dune migration versus fixation—based
38 on continuous environmental predictors. This method was first developed by Hosmer and Lemeshow,
39 (1980) and Lemeshow and Hosmer (1982), and has been successfully applied in related environmental
40 fields to model landslide susceptibility (Ohlmacher and Davis, 2003; Lombardo et al., 2015), soil
41 distribution (Giasson et al., 2006; Abdel-Kader, 2011), vegetation dynamics (Rudgers and Maron, 2003;
42 Andrew et al., 2012; Snedden and Steyer, 2013; Gallego-Fernández et al., 2015), and extreme climatic
43 events on coastal environments (Koerth et al., 2013; Ozbas and Greenberg, 2013; Pour et al., 2014), yet its
44 application to coastal dune mobility remains notably limited. The few existing studies that employ logistic
45 regression in coastal contexts have focused primarily on habitat change (Brus et al., 2016) or storm damage
46 (Ozbas and Greenberg, 2013), rather than on predicting dune activity from routine meteorological data.



47 The potential of logistic regression for dune studies lies in its ability to integrate multiple climatic
48 variables, including wind speed, precipitation, and large-scale atmospheric indices into a single
49 probabilistic framework (Hosmer et al., 2013; Sperandei, 2014). Unlike descriptive indices, a well-
50 calibrated regression model can provide forecast probability of dune activation, offering a more dynamic
51 tool for land management and risk assessment. Moreover, by relying on standard meteorological
52 observations, such models can be applied in data-scarce regions where more complex numerical simulations
53 are not feasible (Michel et al., 2018).

54 This study addresses this methodological opportunity by developing and validating a binomial
55 logistic regression model to predict dune mobility in the coastal dunefields of northeastern Patagonia,
56 Argentina. This region serves as an ideal natural laboratory due to its strong climatic forcing, well-
57 documented aeolian activity (Carbone et al., 2007; Kokot and Favier–Dubois, 2017; Toffani et al., 2024),
58 and availability of long-term meteorological records. The integration of the Southern Annular Mode
59 (SAM), a key driver of extratropical climate variability in the Southern Hemisphere (Fogt and Marshall,
60 2020), further allows us to examine how regional atmospheric circulation patterns influence local dune
61 dynamics.

62 The primary objectives of this work are 1) to develop a predictive logistic regression model that
63 links meteorological variables and climate indices to the probability of dune activation; 2) to validate the
64 model against multi-decadal records of dune migration derived from remote sensing, and 3) to assess the
65 transferability of the modeling framework and its potential for application in other aeolian environments
66 worldwide.

67 By framing our research around methodological innovation, we aim to provide a generalizable,
68 accessible tool for forecasting dune activity—one that complements existing descriptive approaches and
69 supports proactive coastal management in a changing climate. The study of these landforms is important
70 because they constitute the first barrier against storm impacts, protecting coastal communities from extreme
71 events and serving as freshwater reservoirs for nearby populations (Rusticucci et al., 2016; Portz et al.,
72 2021).

73 2. Study area

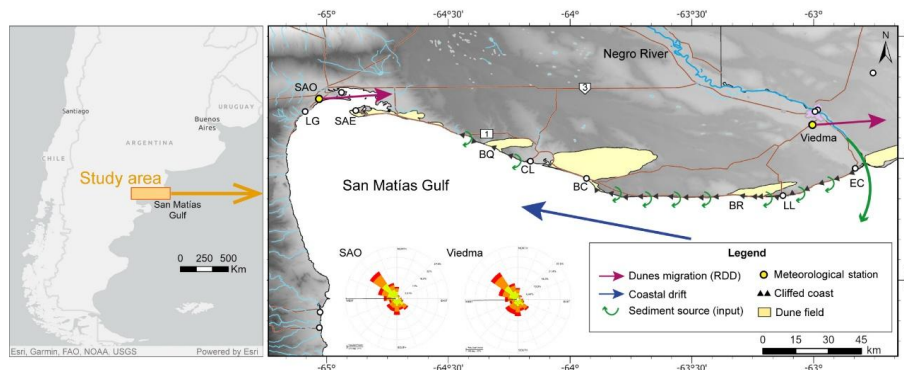
74

75 2.1 Geographic and Demographic Context

76 The study area encompasses the northern coast of the San Matías Gulf, in northeastern Patagonia,
77 Argentina, extending approximately 180 km from the mouth of the Negro River to the town of San Antonio
78 Oeste (SAO) (Fig. 1). This area includes a series of villages and recreational areas, such as El Cóndor, La
79 Lobería, Bahía Rosas, Bahía Creek, Caleta de los Loros, San Antonio Este and Oeste, and Las Grutas
80 (Carbone et al., 2007; Kokot and Favier–Dubois, 2017). The combined permanent population of these
81 towns was 22,205 inhabitants in 2010 (INDEC, 2010), with a significant seasonal increase due to tourism,
82 particularly in Las Grutas, which averaged 118,000 visitors annually between 2006 and 2023 (INDEC,
83 2023). The area is connected by National Route No. 3 and Provincial Route No. 1, the latter running parallel
84 to the coast. The presence of natural protected areas—Bahía de San Antonio, Punta Bermeja, and Pozo
85 Salado–Caleta de Los Loros–Punta Mejillón—highlights the region's ecological value, hosting diverse flora



86 and fauna, as well as archaeological sites evidencing human occupation since at least 6,000 yrs BCE
87 (Favier–Dubois and Kokot, 2011; Marcos and Mancini, 2012; Favier–Dubois, 2013).



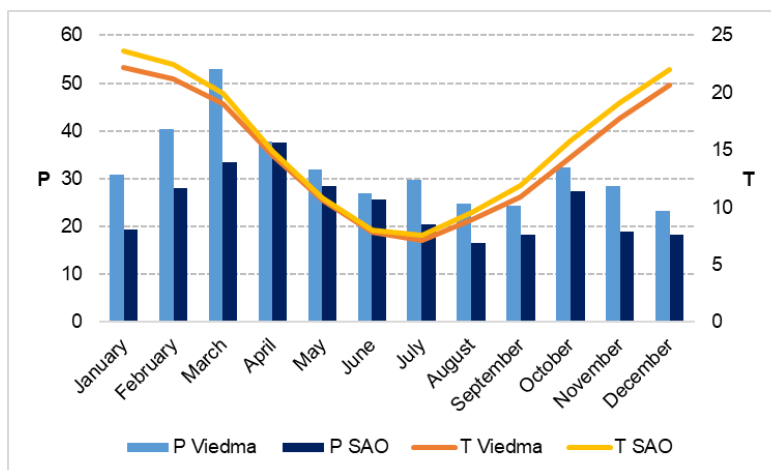
88 **Figure 1. Study area. Meteorological stations, dune fields, and coastal villages. LG: Las**
89 **Grutas, SAO: San Antonio Oeste, SAE: San Antonio Este, BQ: Bajo la Quinta, CL: Caleta de Los**
90 **Loros, BC: Bahía Creek, BR: Bahía Rosas, LL: La Lobería, EC: El Cóndor. SAO and Viedma sand**
91 **roses are present. Argentina map powered by Esri. DEM basemap from Instituto Geográfico**
92 **Nacional.**

93

94 2.2 Climate

95 The climate is classified as cold semi-arid (BSk) according to the Köppen–Geiger system (Peel et
96 al., 2007). Mean annual temperatures range from 14° C to 17° C, with maxima in January (22.2–23.6 ° C)
97 and minima in July (7.1–7.5 °C) (Fig. 2). Annual precipitation increases from west to east, averaging 292
98 mm in SAO and 383 mm in Viedma for the 1991–2020 period, with higher values typically recorded in late
99 summer and autumn (Servicio Meteorológico Nacional [SMN], 2024). Annual evapotranspiration ranges
100 from 1,050 to 1,485 mm, and mean air humidity was 57 % during 1961–2000 (Genchi et al., 2010; Bohn
101 et al., 2014).

102



103 **Figure 2. Mean monthly temperature (° C) and total mean monthly rainfall (mm) between 1991 and**
 104 **2020 registered in Viedma Aero and San Antonio Oeste Aero meteorological stations. P:**
 105 **precipitation; T: temperature.**

106

107 The region lies within the belt of mid-latitude westerlies, driven by the South Pacific and South
 108 Atlantic anticyclones and the subpolar low-pressure channel (del Valle et al., 2008; Rusticucci et al., 2016;
 109 Montes et al., 2017). These winds induce a mean surface circulation towards the E–ENE (Saavedra, 2011;
 110 Pisoni, 2012). Wind speeds are generally highest during the austral summer, exacerbating aridity in an
 111 already dry environment shaped by the rain-shadow effect of the Andes (Montes et al., 2017). Dominant
 112 summer wind directions are W, SW, and NW. Easterly winds, associated with sea breezes, are more
 113 frequent in winter, bringing moisture, cloud cover, and dew (López Alfonsín et al., 2012; Agosta et al.,
 114 2019).

115 The Southern Annular Mode (SAM) is the dominant mode of extratropical climate variability in the
 116 Southern Hemisphere. Its positive phase is associated with a poleward contraction and intensification of
 117 the westerly wind belt, leading to warmer, drier conditions at mid-latitudes (~40° S). Conversely, the
 118 negative phase is characterized by increased precipitation, cooler temperatures, and a northward expansion
 119 of storm tracks (Berman et al., 2012; Fogt and Marshall, 2020). A positive trend in the SAM index has been
 120 observed since the mid-20th century, particularly in summer, linked to greenhouse gas increases and
 121 stratospheric ozone depletion (Fogt and Marshall, 2020).

122 The El Niño–Southern Oscillation (ENSO) also influences regional climate. El Niño events are
 123 typically associated with increased annual precipitation (up to +50 mm) and higher autumn–winter
 124 temperatures in the study area, while La Niña phases correlate with reduced precipitation and cooler
 125 summers (SMN, 2014). The interplay between SAM and ENSO can amplify or attenuate their individual
 126 climatic signals (Rusticucci et al., 2016).

127 The tides in the San Matías Gulf are semidiurnal, with a mean range of 6.67 m at San Antonio Este
 128 and 3.35 m near the Negro River mouth. The maximum high tide reaches 9.62 m and the minimum low
 129 tide is 0.14 m (SHN, 2024). Typical wave heights range from 0.5 to 1.5, reaching up to 3 m during storms,
 130 with periods of 7–10 s (Wörner et al., 2019).



131

132 **2.3 Geology and geomorphology**

133 San Matías Gulf covers approximately 18,000 km² with a maximum depth of 160 m (Isla, 2013).
 134 The gulf was flooded around 11,000 yrs BCE, with the post-glacial marine transgression peak (~6,000 yrs
 135 BCE) reaching about 6 m above present sea level, flooding depressions that now form coastal inlets and
 136 tidal flats (Isla, 1989; Mancini et al., 2005; Favier–Dubois and Kokot, 2011). A subsequent sea-level drop
 137 of 2–4 m, coupled with abundant sand supply and persistent westerlies, favored the development of
 138 extensive transgressive dunefields (Isla, 2013, 2017; Sander et al., 2018). Sand availability has also been
 139 linked to humidity fluctuations over the last 7,500 yrs (Marcos et al., 2014), consistent with typical
 140 formation mechanisms for transgressive coastal dunefields (Hesp, 2013).

141 The northern coast of the gulf features active sea cliffs fronted by beaches, backed by cliff-top dunes
 142 where cliffs are present, and transgressive dunefields where cliffs are absent (Toffani, 2020). Major dune
 143 fields include Bahía Rosas (largely stabilized), Bahía Creek, Bajo la Quinta, San Antonio Oeste/Oeste, and
 144 El Cóndor-Villa 7 de Marzo (Table 1, Fig. 3) (Carbone et al., 2007; Cortizo and Isla, 2012; Kokot and
 145 Favier–Dubois, 2017; Vergara Dal Pont et al., 2017; Sander et al., 2018).

146 The cliffs are composed of sedimentary formations ranging from Oligocene to Holocene age,
 147 including the Gran Bajo del Gualicho, Río Negro, Baliza San Matías, Tehuelche, and San Antonio
 148 formations (Andreis, 1965; Angulo et al., 1978; Lizuain and Sepúlveda, 1978; Sepúlveda, 1983). These
 149 deposits, representing continental and marine facies, are the primary sediment source for the dunes, via cliff
 150 erosion, beach/tidal flat reworking, and dune recycling (Gelós et al., 1990; Zavala and Freije, 2005; Fucks
 151 et al., 2012; Toffani et al., 2020). Sandstone compositions indicate a dominant volcanoclastic contribution
 152 from the North Patagonian Cordillera, mixed with quartz-rich sand derived from the Holocene transgression
 153 and fluvial input from the Negro and Colorado rivers (Gelós et al., 1990).

154

155 **Table 1. Presence or absence of spits, maximum dune width and height, dune migration rate, and**
 156 **direction of the transgressive dune fields within the study area. * No data available. Data sources:**
 157 **San Antonio Oeste (SAO)- San Antonio Este (SAE) (Carbone et al., 2007; Kokot and Favier–Dubois,**
 158 **2017); Bajo la Quinta (Favier–Dubois and Kokot, 2011); Bahía Creek (Sander et al., 2018; Toffani,**
 159 **2020). El Cóndor (Vergara Dal Pont et al., 2017); and Villa 7 de Marzo (Cortizo and Isla, 2012).**

	SAO-SAE	Bajo la Quinta	Bahía Creek	El Cóndor	7 de Marzo
Max width (km)	4	3	14	1	4.5
Max height (m)	10	20	16	6	11
Migration direction	E-NE	ENE	ENE	NE-ENE	NE-ENE
Migration rate (m yr ⁻¹)	4	*	10	7	5-9
Spits	Yes	No	Yes	Yes	Yes

160

161 The dunefields exhibit significant spatial variability in morphology, size, and activity (Table 1, Fig.
 162 3):

163 San Antonio Oeste/Este (SAO/SAE): The dunefield extends up to 4 km in width, featuring
 164 barchanoid and transverse ridges, and blowouts. Dune heights reach up to 10 m, composed of fine to



165 medium sand, migrating at an average rate of 4 m yr^{-1} towards the E–NE (Carbone et al., 2007; Kokot and
166 Favier–Dubois, 2017).

167 Bajo la Quinta: An active dunefield buries Pleistocene–Holocene deposits. Dunes can reach 20 m in
168 height and include barchanoid, transverse, and oblique forms (Favier–Dubois and Kokot, 2011).

169 Bahía Creek–Caleta de Los Loros: This is the largest dunefield in the study area, extending over 36
170 km in length and 5–14 km in width. It features a complex assemblage of crescentic, linear, parabolic,
171 embryo, foredunes, cliff-top, and climbing dunes, with minor occurrences of oblique, reverse, and star
172 dunes. Active dunes cover $\sim 168 \text{ km}^2$, reach heights up to 16 m, migrate ENE at $6\text{--}10 \text{ m yr}^{-1}$, and are
173 composed of medium to fine sand (Sander et al., 2018; Toffani, 2020). Vegetation patches, notably
174 *Sporobolus rigens* and *Hyalis argentea*, form nebkhas.

175 El Cónдор–Villa 7 de Marzo: Near the Negro River mouth, this field consists of barchanoid and
176 parabolic dunes extending 1–4.5 km inland. Migration is towards the NE–ENE at rates of 7 m yr^{-1} (El
177 Cónдор) and $5\text{--}9 \text{ m yr}^{-1}$ (Villa 7 de Marzo) (Cortizo and Isla, 2012; Vergara Dal Pont et al., 2017).

178 This diverse and dynamic coastal setting, with its well-defined climatic forcing, clear sediment
179 sources, and varied dune morphologies, provides an optimal natural laboratory for developing and testing
180 a predictive model of dune mobility based on meteorological parameters.



181 **Figure 3. Main dunefields within the study area. (a): San Antonio Este. (b): Bajo la Quinta. (c): Bahía**
182 **Creek. (d): El Cónдор-Villa 7 de Marzo. Imagery © 2025 Airbus, Map data © 2022–2024 Google.**

183

184 3. Methods

185

186 Climatic data were obtained from the Viedma Aero and San Antonio Oeste Aero (SAO)
187 meteorological stations operated by the SMN. The study period was 1991–2020, during which at least
188 hourly records were collected from 6 a.m. to 11 p.m. This time frame corresponds to a standard reference



189 period for regional climatic studies, as recommended by the World Meteorological Organization (Wang,
190 2005). In Viedma, the data were recorded 7 m above the ground, while in SAO, they were recorded 20 m
191 above the ground. Both datasets were normalized to 10 m standard acquisition data height (Touma, 1977;
192 Robeson and Shein, 1997; Klink, 1999), according to the following Eq. (1) (Guevara Díaz, 2013):

193

$$194 \quad V_z/V_{ref} = (Z/Z_{ref})^a, \quad (1)$$

195

196 where V_z is the wind speed to be estimated at the height (Z), where the measurement was taken; V_{ref} is the
197 measured wind speed; Z_{ref} is the standardized height above the ground; and “ a ” is the wind shear exponent
198 ($a=0.2$ in this study, corresponding to crops and bushes).

199 Hourly wind speed and direction (grouped monthly), total monthly precipitation, and mean monthly
200 temperature data were analyzed. In addition, values for the SAM and the Southern Oscillation Index (SOI)
201 were analyzed, obtained from the Natural Environment Research Council–British Antarctic Survey
202 (NERC–BAS) and the National Oceanic and Atmospheric Administration (NOAA), respectively. Wave
203 height data were downloaded from a Copernicus reanalysis, while cattle population was obtained from
204 several censuses from the Instituto Nacional de Estadística y Censos (INDEC) between 1960 and 2018.

205 Wind speeds exceeding 6.17 m s^{-1} were considered sufficient for sediment transport, based on
206 Toffani’s (2020) calculations, which considered local grain size, environmental conditions, and Bagnold’s
207 (1954) equations for the friction speed threshold, when sediment transport begins and the minimum velocity
208 threshold for grains to travel by saltation. Annual and seasonal DP were calculated according to the formula
209 developed by Fryberger and Dean (1979):

210

$$211 \quad Q \propto V^2(V - V_t) * t, \quad (2)$$

212 where Q represents transported sediments within a certain time t , V is the mean wind speed during t time,
213 V_t is the minimum speed for wind saltation transport, and t is the wind blow time as a percentage. The
214 Fryberger and Dean’s (1979) method was applied using wind velocity data expressed in knots, with 16
215 directional classes based on geographic coordinates (each 22.5°). DP indicates wind energy environments
216 classified as low (<200), mean ($200\text{--}400$), and high (>400). From these, the RDP and RDD were calculated.
217 This approach is commonly used to assess regional wind intensity and sand transport in areas receiving
218 more than 50 mm of annual rainfall (Levin et al., 2014).

219 The Lancaster (1988) and Tsoar (2005) mobility indices were calculated to estimate a measure of
220 dune migration:

221

$$222 \quad M = \frac{DP}{1000 - (750 \frac{RDP}{DP})} \quad (3)$$

223

$$224 \quad M = W/(P/PE) \quad (4)$$

225



226 Equation (3) represents the Tsoar index, which has been widely used to study dune fields across
227 diverse environments worldwide, subjected to different climatic conditions. This index assumes that wind
228 intensity is the most important factor in dune activity and is valid for sites with annual rainfall greater than
229 50 mm. Values below 1 represent fixed or vegetated dunes, whereas values above 1 correspond to dunes
230 that are fully active or lack vegetation growth (Tsoar, 2005). Equation (4) represents the Lancaster index,
231 where W is the wind percentage above the sand transport threshold, P is precipitation, and PE represents
232 potential evapotranspiration, obtained using the Thornthwaite equation (Thornthwaite, 1948). This equation
233 has also been successfully applied to assess dune behavior across different environments. According to
234 Hugenholtz and Wolfe (2005), dunes are classified as inactive when $M < 50$, as active crest dunes when
235 $50 < M < 100$, as active dunes except the interdune area when $100 < M < 200$, and as fully active dunes when
236 $M > 200$. For this study, dunes were considered active only when both the Tsoar index exceeded 1 and the
237 Lancaster index exceeded 50 at the same time. This new index is referred to here as the TsoLa index.

238 Satellite and aerial images were processed to estimate dune migration rates between 1986 and 2023.
239 Visible-spectrum images with a spatial resolution of 1.05 to 1.25 m and three bands, corresponding to the
240 years 2003, 2004, 2009, 2010, 2013, 2016, 2019, 2020, and 2023, were obtained from Google Earth.
241 Additionally, a 1986 aerial image with 2.35 m resolution and three bands was obtained from the Instituto
242 Geográfico Nacional. Due to cloud cover, some dune fronts were not identified in the 2009 image from
243 Viedma. The images were processed using ArcGIS Pro 3.4.0. They were georeferenced using control
244 points, orthorectified, and projected to the WGS84 UTM Zone 20 S coordinate system. Dune fronts and
245 selected precipitation ridges were drawn manually. To quantify migration rates, points were automatically
246 placed at 50 m intervals along the reference line, and orthogonal distances between those points and the
247 subsequent year's dune front position were measured to establish migration rates. The root mean square
248 error (RMSE) values were always below the spatial resolution of the images, indicating minimal position
249 error. Meteorological data from the SAO station were compared with dune activity in the San Antonio Este
250 dunefield, located 13 km away. Likewise, data from the Viedma meteorological station were compared to
251 the El Cóndor-Villa 7 de Marzo dunefield, located 26 km away, distances equal to or less than those
252 considered acceptable by Hugenholtz and Wolfe (2005).

253 For the statistical analysis, RStudio software (version 2024.12.0), including the boot, broom, car,
254 ggeffects, ggplot2, glm2, glm.predict, glmtoolbox, mosaic, ResourceSelection, ROCR, sjPlot, and vcd
255 packages, was used to perform a multiple binary logistic regression, following the guidelines proposed by
256 Hosmer and Lemeshow (1980), Kalil et al. (2010), and Stoltzfus (2011). This statistical method is used to
257 establish the relationship between a set of continuous independent predictor variables and a binary
258 categorical variable to model the probability of occurrence of an event, for which variables with $p < 0.05$
259 were considered significant, represented as $\Pr(>|z|)$ in the software calculations (Zhu, 2016).

260 To perform the logistic regression, the independence of the predictor variables was considered
261 through statistical correlation tests using the "cor.test()" function, with significance defined as $p < 0.05$
262 (Schober et al., 2018). Colinearity was evaluated to exclude correlated variables, seeking values closer to
263 1 (Daoud, 2017). Likewise, the less frequent results concerning the number of independent variables were
264 considered to avoid overfitting (ratio equal to or greater than 10) (Kalil et al., 2010). The outliers were
265 calculated based on the third quartile plus 1.5 times the interquartile range. However, they were retained in



266 the analysis as they were interpreted as valid extreme environmental values rather than measurement errors.
267 Once the individual variables met the selection criteria, they were combined in the model, which was tested
268 using the “stats::step(model)” function to identify if the overall model performed better with or without
269 each variable. Thus, the final models included monthly values (1991–2020) of the SAM index, total
270 monthly precipitation, and monthly average wind speed as independent predictor variables. Temperature,
271 potential evapotranspiration, and soil moisture were excluded due to multicollinearity, while wave height,
272 cattle population, and SOI and NDVI indices were excluded to improve the model performance. Moreover,
273 monthly data for cattle and NDVI were considered unreliable due to limited availability and minimal
274 temporal variability. The binary categorical variable was defined using a combination of the Tsoar and
275 Lancaster indices and RDD values. A value of 0 was assigned when the dunes behaved as fixed in at least
276 one index and/or when the RDD values ranged between 181° and 360°. Conversely, a value of 1 was
277 assigned when they behaved as active in both indices and the RDD values ranged from 1° to 180°, consistent
278 with the general drift direction for dunes along the coast.

279 The estimated probability for each model, known as the Logit function (\hat{p}), is:

280

$$281 \quad \hat{p} = (e^{(\beta_0 + \beta_1 X_1 + \dots + \beta_n X_n)}) / (1 + e^{(\beta_0 + \beta_1 X_1 + \dots + \beta_n X_n)})$$

$$282 \quad = \ln(\hat{p} / (1 - \hat{p})) = \beta_0 + \beta_1 X_1 + \dots + \beta_n X_n, \quad (5)$$

283

284 where X_1, X_2, \dots, X_n are the different predictors and $\beta_1, \beta_2, \dots, \beta_n$ are their associated coefficients
285 (Herrera Briones, 2023). If the regression coefficient β_i is positive (negative), an increase in the
286 explanatory variable X_i increases (decreases) the probability of the event (\hat{p}) (Sperandei, 2014). The inverse
287 function of the Logit is the cumulative distribution function, also known as the sigmoid function, which is
288 used to plot the probabilities of occurrence of an event (Jansche, 2005).

289 To build the statistical model, the dataset was randomly split, allocating 70 % for training and 30 %
290 for testing. The accuracy of the models for both subsets was evaluated by calculating the proportion of
291 correct predictions made by the model relative to the total number of predictions made. To separate these
292 classes, a threshold value was determined that maximized or minimized a specific metric (between 0 and
293 1). This optimal cut-off point was identified using the “opt.cut” function. In this study, priority was given
294 to minimizing false negatives, which correspond to cases where dunes mobility is not predicted despite the
295 actual movement, given the potential risks this poses to nearby coastal villages and for coastal management
296 applications based on coastal dunes dynamics. To achieve this, the cut-off value that maximizes sensitivity
297 (true positive rate) was selected. Additionally, the receiver operating characteristic curve (ROC) and the
298 area under the curve (AUC) value were used to evaluate the model's performance. An AUC value greater
299 than 0.5 indicates that the model performs better than random guessing. However, the model is overfitted
300 when this value is close to 1 (Wei and Dunbrack, 2013).

301 The goodness of fit of the model was evaluated, i.e., how well it can predict whether a dune is fixed
302 or mobile, using the chi-square regression test (with $p < 0.05$ considered statistically significant) (Healy,
303 2006) and the Hosmer–Lemeshow test, where $p > 0.05$ indicates adequate fit (Hosmer and Lemeshow,
304 1980). Finally, internal validation of the predictive values was also performed using a bootstrapping method
305 (Steyerberg et al., 2001).



306 **4. Results**

307

308 According to the established procedures, the optimal model for each location included the Southern
309 Annular Mode (SAM), precipitation, and wind speed as predictor variables. A total of 360 data
310 measurements per variable were used for each meteorological station to develop the models. Overfitting
311 was assessed based on the frequency of the least common outcome relative to the number of independent
312 variables ($n=3$), resulting in at least 30 events of each possible outcome (0 and 1). Variance Inflation Factor
313 (VIF) values were below 1.08 in SAO and below 1.16 in Viedma, indicating no multicollinearity.
314 Precipitation ranged from 122 mm to 578 mm in SAO and from 214 mm to 653 mm in Viedma, while SAM
315 index values varied between -5.77 and 4.92. For wind, a more exhaustive analysis was performed. Winds
316 exceeding the minimum threshold accounted for 33.7 % of the total observations for the 1991–2020 period
317 in SAO and 30.6 % in Viedma, mainly blowing from the NW and SW in both cases. According to the Tsoar
318 index, dunes were identified as active in 119 months (33.1 %) in SAO and in 268 months (74.4 %) in
319 Viedma. Using the Lancaster index, dunes were classified as mobile during 254 months (70.6 %) in SAO
320 and during 247 months (68.6 %) in Viedma. When both indices were considered simultaneously, active
321 dune conditions were recorded in 82 months (22.8 %) in SAO and in 160 months (44.4 %) in Viedma.
322 Monthly DP values in SAO ranged from 30 to 1,976, averaging 549. In Viedma, DP values ranged from 55
323 to 6,203, with a mean of 1,176 (Fig. 4). Overall, higher DP values were recorded during the austral summer,
324 with NW, SW, and SE as main components, while lower values were typical in autumn. During the
325 remainder of the year, most records correspond to the NW component, with the addition of the SW
326 component during spring in Viedma, where in general stronger winds were registered (Fig. 5). The RDD
327 values suggest a general trend of dune migration toward the east. Over the full study period, the mean RDD
328 was 90° in SAO and 89° in Viedma. A decreasing trend in DP values was observed in Viedma over time
329 (Fig. 6). In contrast, although fluctuations were recorded in SAO, DP values remained relatively stable over
330 the study period (Fig. 6). RDP values generally follow these tendencies.

331

332

333

334

335

336

337

338

339

340

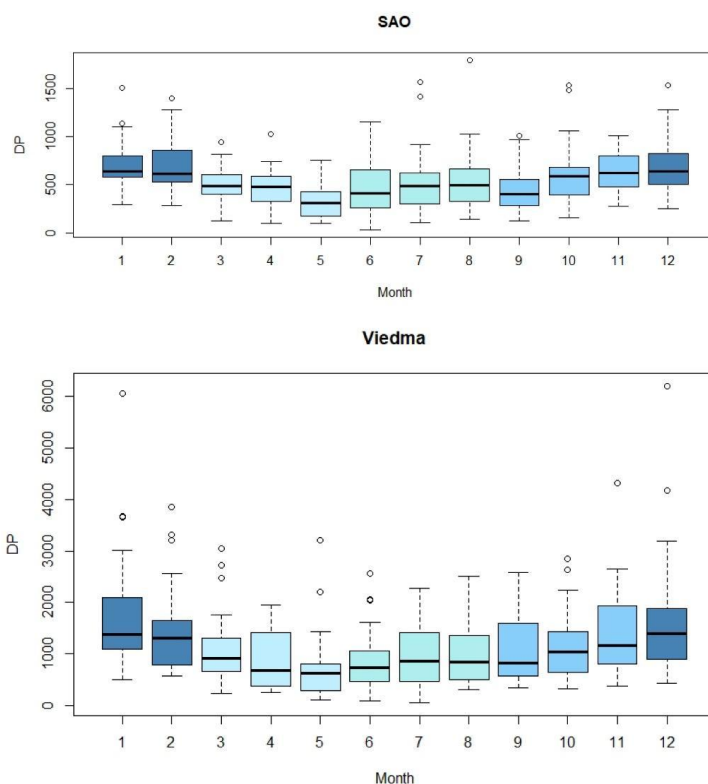
341

342

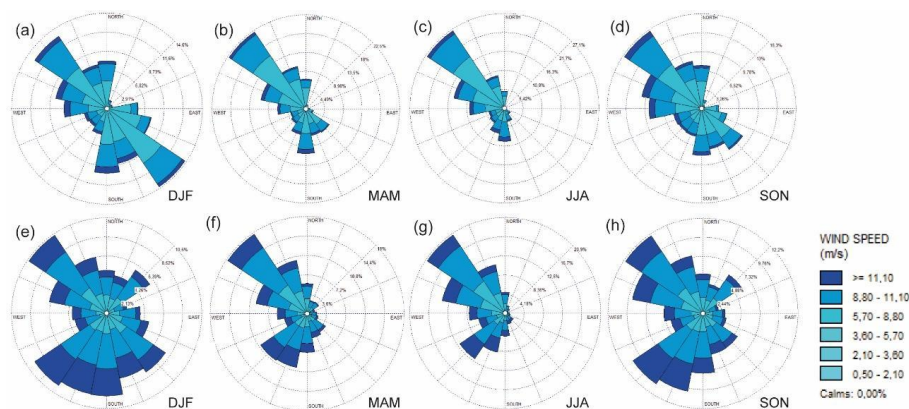
343

344

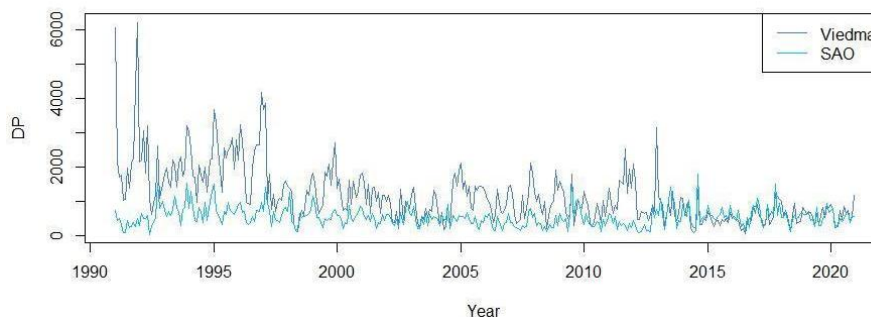
345



346 **Figure 4. Boxplots showing the monthly Drift Potential values obtained from SAO and Viedma**
 347 **meteorological stations during the 1991–2020 period.**
 348



349 **Figure 5. Seasonal winds above the sediment transport threshold for the 1991-2020 period. (a-**
 350 **d): San Antonio Oeste, (a): summer, (b): fall, (c): Winter, (d): spring. (e-h): Viedma, (e): summer, (f):**
 351 **fall, (g): winter, (h): spring.**
 352



353
354 **Figure 6. Drift Potential variation between 1991 and 2020, according to the recorded winds in Viedma**
355 **and SAO.**

356 For both study areas, the logistic regression model identified three significant predictors of dune
357 migration: SAM, precipitation (P), and wind speed (Wind) (Table 2). In the SAO region, significance levels
358 were $p = 0.01$ for SAM, $p = 0.001$ for precipitation, and $p < 0.001$ for wind speed. In Viedma, all three
359 predictors also showed statistical significance ($p = 0.04$ for SAM, $p < 0.001$ for precipitation, and $p < 0.001$
360 for wind speed). The estimated coefficients indicate that SAM and precipitation have a negative effect on
361 dune migration probability, while wind speed has a positive effect. This suggests that the probability of
362 dune migration (i.e., the event coded as 1) increases when wind speeds are higher or if precipitation and
363 SAM index values decrease. Coefficient values further support this interpretation: in the SAO region,
364 estimates were -0.3 for SAM, -0.04 for precipitation, and 0.64 for wind speed; in Viedma, the values were
365 -0.2 , -0.04 , and 0.32 , respectively. The combined influence of these three variables determines the final
366 predicted probability of dune migration for each observation (Table 2). A response curve was generated to
367 visualize these relationships (Fig. 7), illustrating that dune migration is unlikely when precipitation exceeds
368 150 mm , wind speeds fall below 20 km h^{-1} , or SAM values are high.

369
370 **Table 2. SAO and Viedma logistic regression estimates (log-odds), 95% confidence intervals (CI),**
371 **and p-values are shown for each predictor. $p < 0.05$ values result significant to the model.**

TsoLa San Antonio Oeste			
Predictors	Estimate	CI	p
(Intercept)	-14.52	-19.17 – -10.57	<0.001
SAM	-0.30	-0.54 – -0.07	0.011
Precipitation	-0.04	-0.06 – -0.02	0.001
Wind	0.64	0.46 – 0.84	<0.001

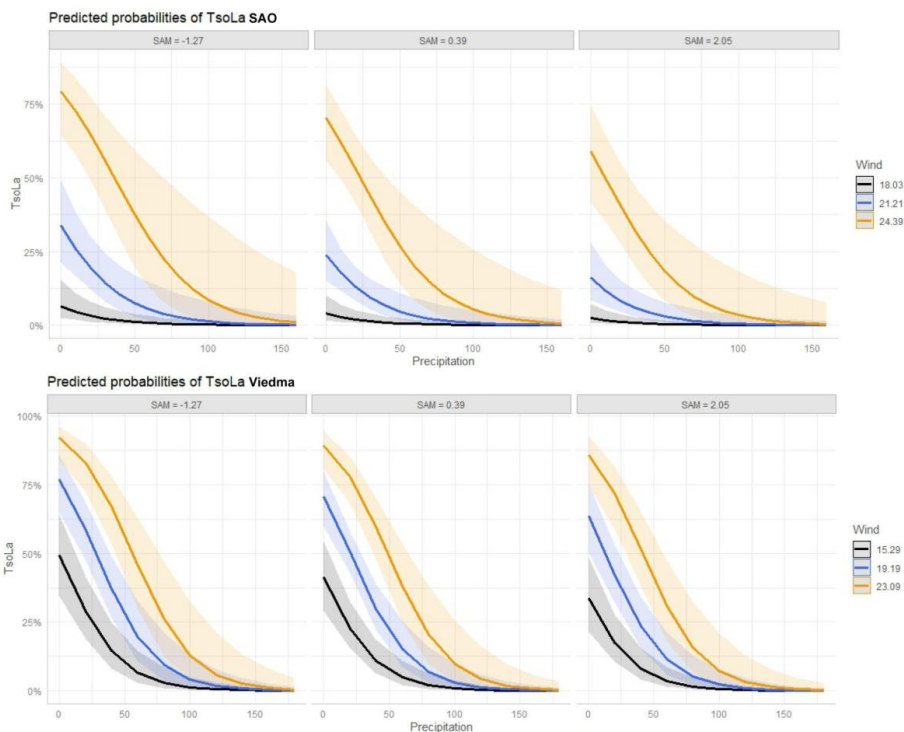
372

TsoLa Viedma			
Predictors	Estimate	CI	p
(Intercept)	-5.15	-7.03 – -3.42	<0.001
SAM	-0.20	-0.39 – -0.01	0.040
Precipitation	-0.04	-0.06 – -0.03	<0.001



Wind	0.32	0.23 – 0.42	<0.001
------	------	-------------	--------

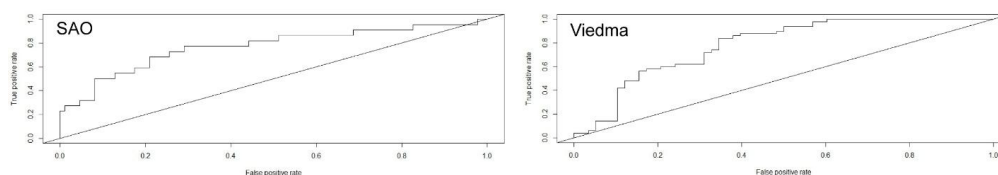
373



374 **Figure 7. The plots show how the TsoLa probability diminishes when precipitation increases and**
 375 **wind speed is slower for different SAM values in both meteorological stations. SAO curves on top,**
 376 **Viedma curves at the bottom.**

377

378 The logistic regression models demonstrated a good fit, as indicated by the likelihood ratio test ($p <$
 379 0.001) and the Hosmer–Lemeshow goodness-of-fit test ($p > 0.05$). These results suggest that the models
 380 adequately represent the relationship between the predictor variables and dune migration probability. Model
 381 discrimination was further assessed using the Area Under the Receiver Operating Characteristic Curve
 382 (AUC-ROC), which yielded values of 0.77 for SAO and 0.78 for Viedma, indicating acceptable predictive
 383 performance. The optimal classification thresholds (cut-points) were determined to be 0.8 for SAO and 0.4
 384 for Viedma (Fig. 8).



385

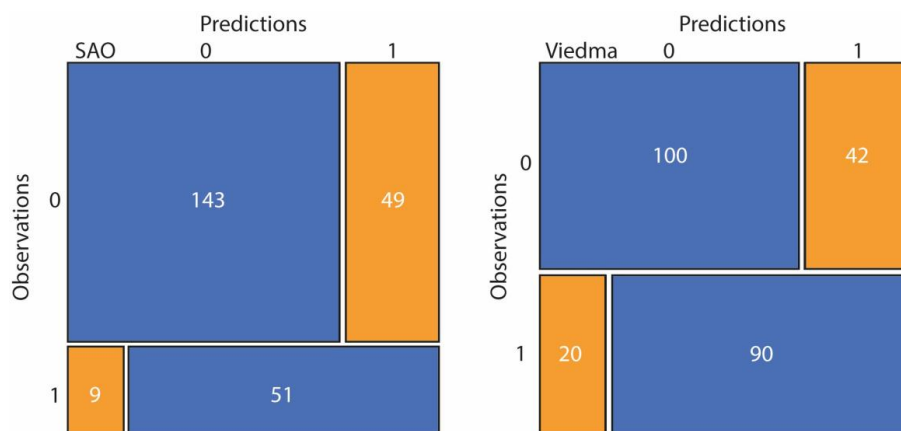


386 **Figure 8. Area Under the Receiver Operating Characteristic (AUC-ROC) curves for SAO (left) and**
 387 **Viedma (right).**

388

389 The models also showed consistent classification performance. In SAO, the model correctly
 390 classified 77 % of the training data and 73 % of the test data, while in Viedma, 75 % of the training and
 391 74% of the test observations were correctly predicted (Figs. 9–10). A breakdown of classification
 392 performance shows that, for the training data, in SAO, predictions included 57 % true negatives, 20 % true
 393 positives, 19 % false positives, and 4 % false negatives (Fig. 9). In Viedma, the distribution was 39 % true
 394 negatives, 36 % true positives, 17 % false positives, and 8% false negatives (Fig. 9). For the test data in
 395 SAO, dunes were correctly classified as active in 15 % of cases and as fixed in 58 %. False positives
 396 accounted for 21 %, and false negatives for 5 % (Fig. 10). In Viedma, dunes were correctly predicted as
 397 active in 39 % of cases and fixed in 35 %. False positives represented 7 %, while false negatives reached
 398 19 % (Fig. 10).

399



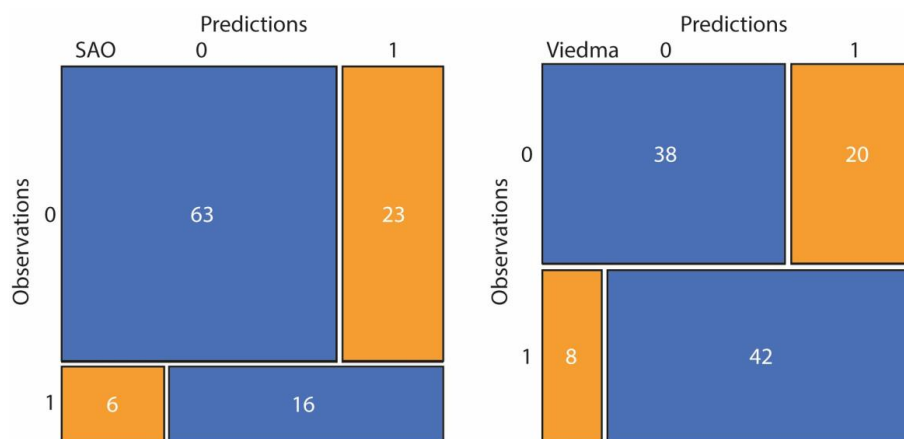
400 **Figure 9. Confusion matrix for the training data in SAO (left) and Viedma (right).**

401

402 A bootstrap analysis with 1,000 resample attempts with replacement was performed to validate the
 403 stability of the fitted logistic regression model. The model coefficients were estimated in each iteration. In
 404 SAO, the coefficient associated with the variable Wind had a mean value of 0.635, with a 95 % confidence
 405 interval (percentile method) of [0.421, 0.806], suggesting a positive and consistent effect on the probability
 406 of TsoLa occurrence. In contrast, SAM and Precipitation showed negative effects, with average bootstrap
 407 coefficients of -0.296 and -0.037, and respective 95 % confidence intervals of [-0.553, -0.035] and [-0.060,
 408 -0.017]. In Viedma, the coefficient associated with the variable Wind had a mean value of 0.318, with a 95
 409 % confidence interval (percentile method) of [0.218, 0.427]; the coefficient associated with the variable
 410 SAM had a mean value of -0.196, with a 95 % confidence interval of [-0.379, -0.035]; and the coefficient
 411 related to the variable Precipitation showed a mean value of -0.044, with a 95 % confidence interval of [-
 412 0.059, -0.029]. This non-parametric approach enabled a robust assessment of predictor significance without
 413 relying on classical model assumptions.



414



415 **Figure 10. Confusion matrix for the test data in SAO (left) and Viedma (right).**

416

417

418

419

420

421

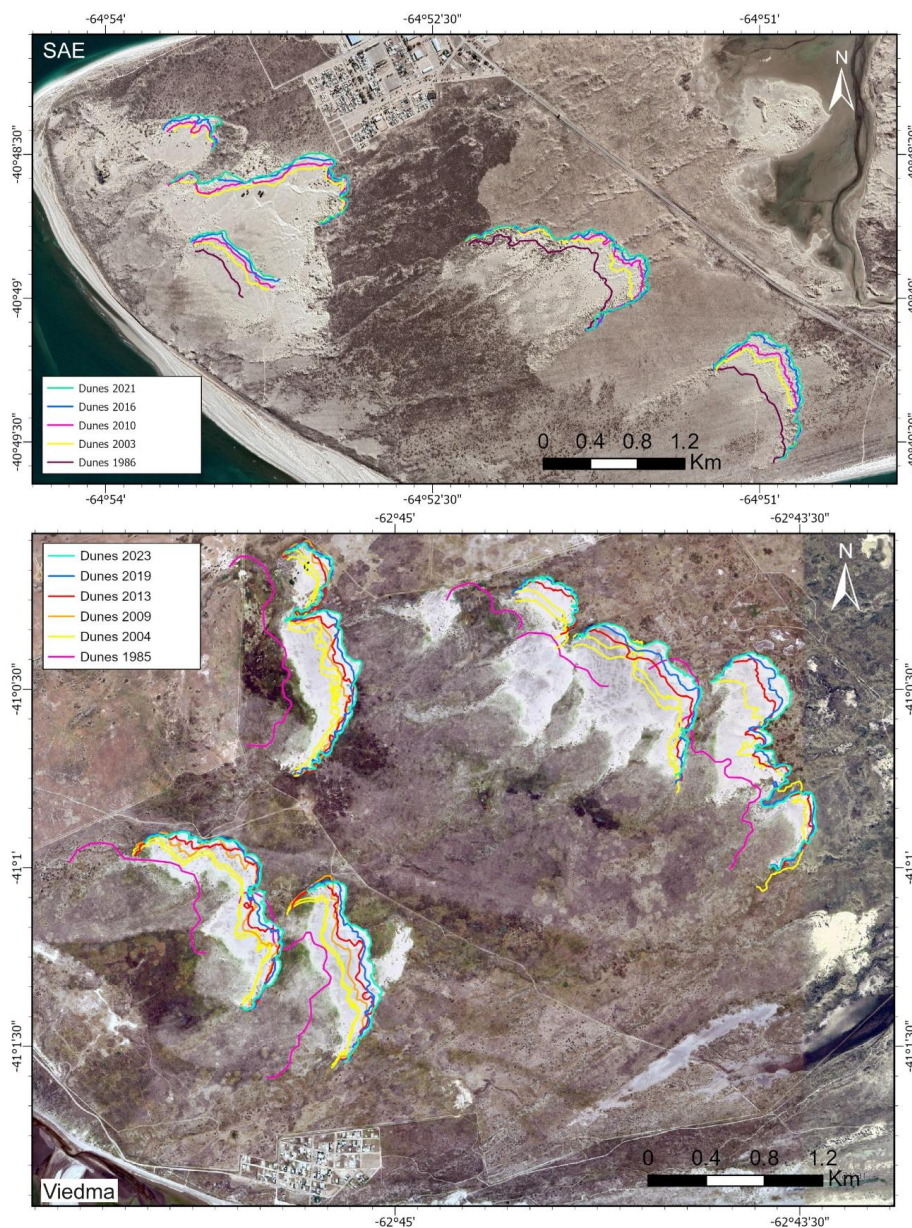
422

423

424

425

To estimate dune migration over time, different dune fronts from the San Antonio area (1986–2021) and the Viedma/El Cóndor-Villa 7 de Marzo area (2003–2023) were studied (Fig. 11). The dune precipitation ridge was measured at a minimum of 20 points per dune/dunefield for each specific time period. In San Antonio, average migration rates ranged from 2.51 to 6.01 m yr⁻¹ (Table 3), with no significant correlation to RDP values, except for one dune (R=0.71). In contrast, in Viedma, the average migration ranged from 2.92 to 10.12 m yr⁻¹ (Table 3), showing a general decreasing trend over time and a positive correlation with RDP values for the same periods, R = 0.84 (Table 3). The RDP values were selected because they better represent the wind intensity in relation to the direction of dune migration.



426 Figure 11. Dune migration between 1985 and 2023 in the San Antonio Este (SAE) area and the
 427 Viedma–Villa 7 de Marzo areas. Imagery © 2025-2026 CNES/Airbus and Maxar Technologies, Map
 428 data © 2003-2023 Google.

429

430 Table 3. Dune migration rates and average RDP values for the 1991-2020 period.

SAO		1986-2003	2003-2010	2010-2016	2016-2021	R2
	Dune 1	-	2.43	4.45	3.66	0.71



	Dune 2	-	3.29	4.11		1.63	0.12
	Dune 3	5.85	5.85	5.22		4.55	0.18
	Dune 4	5.31	3.52	2.43		0.82	0.01
	Dune 5	6.86	3.81	5.40		1.90	0.07
	Mean	6.01	3.78	4.32		2.51	0.07
	RDP	276.75	233.3	264.92		271.73	-
Viedma		1985-2004	2004-2009	2009-2013	2013-2019	2019-2023	R2
	Dune 1	12.26	8.39	2.53	2.42	2.16	0.74
	Dune 2	9	9.37	4.3	3.57	2.31	0.54
	Dune 3	9.52	9.97	4.32	4.02	5.19	0.46
	Dune 4	8.22	5.01		5.26	4.06	0.81
	Dune 5	8.73	5.77		2.56	0.42	0.84
	Dune 6	13.02	3.6		2.94	3.37	0.88
	Mean	10.12	7.02	4.26	3.46	2.92	0.84
RDP	718.84	483.94	503.83	336.07	374.65	-	

431

432

5. Discussion

433

434

435

436

437

438

439

440

441

442

443

444

445

446

447

448

449

450

451

452

453

454

455

456

The statistical significance of wind speed as a predictor of the binomial outcomes of the TsoLa mobility index supports the model’s validity. Ultimately, the values of this index are related to this parameter through the DP and RDP values, as defined by the formula used in its calculation. Furthermore, the dominance of the westerlies is reflected in the RDD values. The observed negative relationship between precipitation and dune migration direction may be attributed to increased soil moisture resulting from higher precipitation levels, which restricts dune mobility and promotes their fixation. Additionally, easterly winds (SE) of oceanic origin are typically associated with greater moisture influx inland and increased precipitation. This pattern is consistent with the findings reported by Agosta et al. (2019), especially during austral fall and winter. Both factors influence general dune migration towards ENE, because easterly wind components are less frequent and are usually associated with rainfall, which decelerates dune migration. Finally, the negative estimate value of the SAM in the model can be attributed to its climatological implications. Negative SAM phases are associated with a northward displacement of the mid-latitude westerlies, bringing stronger winds, lower temperatures, and increased precipitation to regions around 40° S. Although precipitation increases slightly, heightened storm activity and lower temperatures are often associated with greater instability in coastal dune fields and the destabilization of vegetated dunes (Jackson et al., 2019a; 2019b). Conversely, during positive SAM phases, the atmospheric circulation shifts southward, leading to more stable weather, weaker winds, higher temperatures, and reduced precipitation in the study area. These conditions generally favor vegetation growth and dune stabilization (Toffani et al., 2024). This highlights the dominant role of wind over precipitation in controlling sediment transport, reinforcing wind as the primary driver of dune mobility. It is also worth to mention that the DP shows a tendency toward higher values during warmer months, likely reflecting periods with longer daylight hours, higher temperatures, and stronger winds. These features favor the drying of the material that may be transported by winds, even though torrential rains can occur.



457 Considering these parameters together with the general decline in dune migration rates, the observed
458 trend can be linked to a progressive greening of the landscape. This process is characterized by increasing
459 vegetation cover and dune fixation due to weaker winds (reflected in lower values of DP and RDP), higher
460 temperatures, and a trend to more positive SAM index values (Toffani et al., 2024). These changes are more
461 pronounced in Viedma. In San Antonio, the slower dune migration rates may be related to dune morphology
462 and sand supply: shorter and “worm-like” dunes there appear to experience faster vegetation colonization
463 (Toffani et al., 2024). Combined with lower sediment supply and wind intensity, vegetation colonization
464 may result in slower dune migration rates not necessarily directly related to the RDP. Therefore, dune
465 stabilization can occur over decadal timescales (i.e., 10 to 20 years) (Delgado–Fernández et al., 2019;
466 Jackson et al., 2019a). Even if wind speed increases, enhanced vegetation cover and dune fixation may
467 prevent increases in dune migration, indicating that the RDP value alone does not fully reflect dune mobility
468 dynamics, being dune mobility also limited by sediment supply. Contrarily, the Viedma area has a greater
469 sand supply due to its proximity to the mouth of the Negro River, allowing the growth of larger transverse
470 dunes, with their migration controlled by transport capability, reflected in the correlation to RDP values.
471 San Antonio receives sand primarily from its narrow adjacent beach and the San Antonio Bay, resulting in
472 a more limited sand budget (Carbone et al., 2007). This contrast highlights the importance of integrating
473 geological and geomorphological variables into predictive models. In addition, mean dune migration rate
474 values are higher in Viedma than in SAE, related to more intensive winds and higher DP and RDP values
475 in the region.

476 The absence of a significant effect of the regional climate index SOI and the relatively minor
477 influence of SAM compared to precipitation and wind speed in the models may be attributed to a stronger
478 influence of local-scale phenomena driving dune dynamics. The exclusion of SOI is justified by its
479 negligible contribution to the model. SOI reflects conditions associated with El Niño and La Niña events,
480 which in the study area result in relatively minor climatic anomalies: annual precipitation variations of no
481 more than 50 mm and temperature deviations typically below $\pm 0.5^\circ$ C. However, some authors have
482 reported delayed effects of El Niño over southeastern South America, which may help explain the limited
483 influence of this variable in the current analysis. The reported lag period varies between 5 months in Buenos
484 Aires and 8-13 months in southernmost Patagonia (Schneider and Gies, 2004; Pasquini et al., 2008). Further
485 work is needed to obtain a correct lag period for the SAO and Viedma areas.

486 The AUC values obtained for the model, 0.77 for SAO and 0.78 for Viedma, indicate a good fit and
487 suggest that the selected predictors can be considered reliable indicators of dune migration dynamics. The
488 distribution of true positives and true negatives confirms that the models perform reasonably well,
489 particularly in identifying stable dune conditions. The Viedma model shows a higher rate of false positives
490 in the test dataset, indicating some limitations in detecting fixed dunes. This reflects the chosen optimum
491 cut value, which prioritizes minimizing false negatives. Despite these strengths, model performance is
492 constrained by the limited number of observations, i.e., 360 records per station. While this sample dataset
493 is sufficient to detect general patterns, the lower number of positive cases in SAO restricts the model's
494 robustness. For those cases, data covering more years can help to improve it. Furthermore, given the values
495 of each variable, it is possible to estimate what values of the remaining variables are needed to get a higher
496 or lower chance of dune migration.



497 With improved datasets, such as higher-resolution livestock data, vegetation index, sediment supply,
498 or wave dynamics, a more accurate and representative model could be developed, allowing for better
499 predictive capabilities. In this study, wave data were obtained from reanalysis sources; however, this
500 variable could be refined using data from nearby buoys. Livestock data are limited to annual records at
501 different governmental agencies, rather than at localized scales near the dune fields. Monthly vegetation
502 indices have poor spatial resolution, with similar values for each month. This lack of variation may be
503 associated with the low resolution or minimal change in vegetation cover over time. Finally, the absence of
504 a reliable method to estimate monthly sediment supply remains a significant gap and its inclusion would
505 substantially improve the model performance. Nevertheless, the current model demonstrates that even with
506 basic meteorological data from standard weather stations, a Binomial Logistic Regression Model can
507 provide a reasonably robust prediction of dune mobility. The development and application of such models
508 is crucial, given that these phenomena already impact, and will continue to impact, nearby populations.
509 Predictive modeling supports more informed and proactive land-use planning and decision-making policies,
510 particularly in coastal areas experiencing population growth and infrastructure expansion. These models
511 gain even greater relevance when combined with field-based observations of dune migration. Incorporating
512 data from additional meteorological stations, integrating reanalysis datasets, and/or adding adjusted early
513 mentioned parameters would further refine and strengthen the model's accuracy. Building comparable
514 models for other coastal or inland regions and including other phenomena may enhance their validity.

515 The results derived from the DP analysis herein are consistent with findings from other areas along
516 the Argentine coast and Patagonia, including those obtained by Cortizo and Isla (2012) in the south of the
517 Buenos Aires province, where westerly winds also predominate. There, spring and summer exhibit the
518 highest wind intensity, with average DP values around 900 units. Del Valle et al. (2008), in Peninsula
519 Valdés, obtained higher DP values, comparable to the highest values observed at the Viedma
520 meteorological station. The RDD values also suggest predominantly westerly winds throughout the entire
521 year, particularly influenced by the SW and N components. In southern Patagonia, Montes et al. (2015)
522 analyzed the migration rate and direction of certain dunes, which were between 29.6 and 70 m yr⁻¹ and
523 towards the E (86° N) between 2003 and 2013 in the central area of the San Jorge Gulf. Additionally, at a
524 site adjacent to Colhué Huapi Lake, Montes et al. (2017) recorded an average dune advance of 45 m yr⁻¹
525 towards the E (95° N). These places exhibit similar dynamics and could serve to upgrade the model and
526 extend it to inland dunes.

527 **6. Conclusions**

528 This study demonstrates that binomial logistic regression provides a robust and transferable
529 methodological framework for predicting coastal dune mobility based on standard meteorological variables.
530 By integrating established wind-based indices (DP, RDP) with a novel mobility index (TsoLa), we
531 developed a probabilistic model that successfully links climatic drivers to discrete geomorphic states (active
532 vs. fixed). The model's strong performance (AUC > 0.75) across two distinct dunefields in NE Patagonia
533 validates its core premise: even with readily available climatic data, it is possible to move beyond



534 descriptive wind roses and mobility indices toward a predictive, probabilistic understanding of dune
535 activity.

536 Our analysis identified wind speed as the primary and most consistent predictor of dune activation,
537 a finding that reinforces the fundamental role of aeolian forcing in dune dynamics while also providing
538 internal validation for the model's logical coherence. The negative relationships with both precipitation and
539 the Southern Annular Mode (SAM) highlight the moderating effects of moisture availability and large-scale
540 atmospheric circulation. Specifically, the SAM's significant role underscores how regional climate modes
541 can exert a measurable, predictable influence on local-scale geomorphic processes—an important linkage
542 for forecasting dune behavior under future climate scenarios.

543 The use of common meteorological parameters (wind speed, precipitation) and globally available
544 climate indices (e.g., SAM, ENSO) means the framework can be adapted to other coastal and inland aeolian
545 systems with minimal modification. While applied here in a semi-arid, wind-driven setting, the model
546 structure can accommodate additional site-specific variables such as vegetation indices (NDVI), sediment
547 supply estimates, or anthropogenic factors where data resolution permits.

548 Notably, the model offers a practical, low-cost tool for land-use planning and proactive coastal
549 zone management. By outputting a probability of dune activation, it enables early identification of periods
550 and locations with higher erosion or encroachment risk, supporting decision-making for infrastructure
551 protection, especially in developing coastal regions vulnerable to climate pressures.

552 Future research should focus on enhancing the model's spatial and temporal resolution, testing its
553 performance in diverse climatic and geomorphic settings (e.g., temperate coastal dunes, arid continental
554 ergs), and incorporating lagged effects of climate oscillations. The integration of higher-frequency remote
555 sensing data, improved sediment budget constraints, and process-based validation using computational
556 fluid dynamics or cellular automata models will further strengthen the predictive power and physical
557 grounding of this statistical approach. Ultimately, this work establishes a scalable pathway for integrating
558 climatic forecasting with geomorphic hazard assessment, contributing to more resilient management of
559 dynamic dune landscapes worldwide.

560

561 **Author contribution:**

562 MT conceptualization, data curation, formal analysis, investigation, methodology, software, visualization,
563 and writing (original draft preparation). SC funding acquisition, investigation, resources, supervision,
564 validation, and writing (review and editing).

565

566 The authors declare that they have no conflict of interest.

567

568 **Acknowledgements**

569 The authors would like to thank Dr. Alina Shechetkina for improving the English language of the
570 manuscript.

571

572 **Financial support**

573 The present work has no specific financial support.



574

575 **References**

576 Abdel-Kader, F. H.: Digital soil mapping at pilot sites in the northwest coast of Egypt: A multinomial
577 logistic regression approach, *Egypt. J. Remote Sens. Space Sci.*, 14(1), 29–40,
578 <https://doi.org/10.1016/j.ejrs.2011.04.001>, 2011.

579 Agosta, E.A., Martin, P.B., and Serio, L.A.: Persistent easterly winds leading to precipitation in the Atlantic
580 Coast of Patagonia, *Int. J. Climatol.*, 39, 5063–5090, <https://doi.org/10.1002/joc.6127>, 2019.

581 Andreis, R.R.: Petrografía y paleocorrientes de la Formación Río Negro (tramo General Conesa-boca del
582 Río Negro), *Rev. Mus. La Plata*, 36, 245–310, <http://sedici.unlp.edu.ar/handle/10915/144048>,
583 1965.

584 Andrew, R. L., Ostevik, K. L., Ebert, D. P., and Rieseberg, L. H.: Adaptation with gene flow across the
585 landscape in a dune sunflower, *Mol. Ecol.*, 21, 2078–2091, <https://doi.org/10.1111/j.1365-294X.2012.05454.x>, 2012.

587 Angulo R., Fidalgo F., Gómez Peral M. A. and Schnack E. J.: Las ingresiones marinas cuaternarias en la
588 bahía de San Antonio y sus vecindades, provincia de Río Negro, 7º Congreso Geológico
589 Argentino, Neuquén, Argentina, April 1978, 271–283, 1978.

590 Bagnold, R. A.: Experiments on a gravity-free dispersion of large solid spheres in a Newtonian fluid under
591 shear. *Proc. R. Soc. Lond., A* 225, 49–63, <https://doi.org/10.1098/rspa.1954.0186>, 1954.

592 Berman, A. L., Silvestri, G., and Compagnucci, R.: Eastern Patagonia seasonal precipitation: influence of
593 southern hemisphere circulation and links with subtropical South American precipitation. *J.*
594 *Clim.*, 25, 6781–6795, <https://doi.org/10.1175/JCLI-D-11-00514.1>, 2012

595 Bohn, V.Y., Sánchez, R.M., Carrascal, C.N., and Romagnoli, F.B.: Estudio preliminar de variables
596 climatológicas y productividad de los suelos, XXIV Congreso Argentino de la Ciencia del Suelo,
597 Bahía Blanca, Argentina, May 2014, 1–6, 2014.

598 Brus, D. J., Slim, P. A., Gort, G., Heidema, A. H., and Van Dobben, H.: Monitoring habitat types by the
599 mixed multinomial logit model using panel data. *Ecol. Indic.*, 67, 108–116,
600 <http://dx.doi.org/10.1016/j.ecolind.2016.02.043>, 2016.

601 Carbone, M.E., Perillo, G.M.E., and Piccolo, M.C.: Dinámica morfológica de los ambientes costeros de
602 Bahía San Antonio Oeste, provincia de Río Negro, *Geoacta* 32, 83–91, ISSN: 0326-7237, 2007.

603 Cortizo, L.C., and Isla, F.I.: Dinámica de la barrera medanosa e islas de barrera de Patagones (Buenos
604 Aires, Argentina). *Lat. Am. J. Sedimentol. Basin Anal.*, 19, 47–63, ISSN 1851-4979, 2012.

605 Daoud, J. I.: Multicollinearity and regression analysis, *J. Phys.: Conf. Ser.* 949, 012009,
606 <https://doi.org/10.1088/1742-6596/949/1/012009>, 2017.

607 Delgado-Fernández, I., O’Keeffe, N., and Davidson-Armott, R.G.: Natural and human controls on dune
608 vegetation cover and disturbance, *Sci. Total Environ.*, 672, 643–656,
609 <https://doi.org/10.1016/j.scitotenv.2019.03.494>, 2019.

610 Favier-Dubois, C.: Hacia una cronología del uso del espacio en la costa norte del golfo San Matías (Río
611 Negro, Argentina): sesgos geológicos e indicadores temporales, in: *Tendencias teórico-*
612 *metodológicas y casos de estudio en la arqueología de la Patagonia*, edited by Zangrando, A.,
613 Barberena, R., Gil, A., Neme, G., Giardina, M., Luna, L., Otaola, C., Paulides, S., Salgán, L., and



- 614 Tivoli, A., Museo de Historia Natural de San Rafael, San Rafael, Argentina, 87–96, 2013.
- 615 Favier–Dubois, C.M., and Kokot, R.: Changing scenarios in Bajo de la Quinta (San Matías Gulf, Northern
616 Patagonia, Argentina): Impact of geomorphologic processes in subsistence and human use of
617 coastal habitats, *Quat. Int.*, 245, 103–110, <https://doi.org/10.1016/j.quaint.2011.03.051>, 2011.
- 618 Fogt, R.L., and Marshall, G.J.: The Southern Annular Mode: variability, trends, and climate impacts across
619 the Southern Hemisphere, *Rev. Clim. Chang.*, 11, e652 <https://doi.org/10.1002/wcc.652>, 2020.
- 620 Fryberger, S.G., and Dean, G.: Dune forms and wind regime, in: *A Study of Global Sand Seas*, edited by
621 McKee, E.D., United States Geological Survey, Washington D.C., 137–169, 1979.
- 622 Fucks, E.E., Schnack, E.J., and Charó, M.: Aspectos geológicos y geomorfológicos del sector N del golfo
623 San Matías, Río Negro, Argentina. *Rev. Soc. Geol. Esp.*, 25, 95–105, 2012.
- 624 Gallego–Fernández, J. B., Muñoz-Valles, S., and Dellafiore, C. M.: Spatio-temporal patterns of
625 colonization and expansion of *Retama monosperma* on developing coastal dunes, *J. Coast.*
626 *Conserv.*, 19, 577–587, <https://doi.org/10.1007/s11852-015-0408-6>, 2015.
- 627 Gao, J., Kennedy, D.M., and McSweeney, S.: Patterns of vegetation expansion during dune stabilization at
628 the decadal scale. *Earth Surf. Process. Landf.*, 48, 3059–3073. <https://doi.org/10.1002/esp.5681>,
629 2023.
- 630 Gelós, E. M., Spagnuolo, J. O., and Schillizzi, R. A.: Caracteres texturales y mineralógicos de sedimentos
631 de playa de la costa norte del golfo San Matías, *Rev. Asoc. Arg. Mineral. Petrol. y Sedimentol*,
632 21, 41–52, 1990.
- 633 Genchi, S.A., Carbone, M.E., Piccolo, M.C., and Perillo, M.E.: Déficit hídrico en San Antonio Oeste,
634 Argentina, *Rev. Climatol.*, 10, 29–43. ISSN 1578-8768, 2010.
- 635 Giasson, E., Clarke, R. T., Inda Junior, A. V., Merten, G. H., and Tornquist, C. G.: Digital soil mapping
636 using multiple logistic regression on terrain parameters in southern Brazil, *Sci. Agric*, 63, 262–
637 268, <https://doi.org/10.1590/S0103-90162006000300008>, 2006.
- 638 Guevara Díaz, J.M.: Cuantificación del perfil del viento hasta 100 m de altura desde la superficie y su
639 incidencia en la climatología eólica, *Terra* 29, 81–101, ISSN 1012-7089, 2013.
- 640 Healy, L. M.: *Logistic regression: An overview*, Eastern Michigan College of Technology, 2006.
- 641 Herrera Briones, J.: *Aplicación de Regresión Logística al análisis de gravedad de lesiones en colisiones de*
642 *vehículos para ensayos experimentales*, M. S. thesis, Universidad Politécnica de Madrid, Spain,
643 147 pp., 2023.
- 644 Hesp, P. A.: Conceptual models of the evolution of transgressive dune field systems, *Geomorphology*, 199,
645 138–149, <https://doi.org/10.1016/j.geomorph.2013.05.014>, 2013.
- 646 Hesp, P.A., and Thom, B.G.: *Geomorphology and evolution of transgressive dunefields*, in: *Coastal Dunes:*
647 *Processes and Morphology*, edited by: Nordstrom, K., Psuty, N., and Carter, W., Wiley and Sons,
648 London, 253–288, 1990.
- 649 Hesp, P.A., DaSilva, M., Miot da Silva, G., Bruce, D., and Keane, R.: Review and direct evidence of
650 transgressive aeolian sand sheet and dunefield Initiation, *Earth Surf. Process. Landf.*, 47, 2660–
651 2675. <https://doi.org/10.1002/esp.5400>, 2022.
- 652 Hoover, R. H., Gaylord, D. R., and Cooper, C. M.: Dune mobility in the St. Anthony Dune Field, Idaho,
653 USA: effects of meteorological variables and lag time, *Geomorphology*, 309, 29–37.



- 654 <https://doi.org/10.1016/j.geomorph.2018.02.018>, 2018.
- 655 Hosmer, D. W., and Lemeshow, S.: Goodness of fit tests for the multiple logistic regression model,
656 *Commun. Stat.–Theor. Meth.*, 9, 1043–1069. <https://doi.org/10.1080/03610928008827941>, 1980.
- 657 Hosmer, D. W., Lemeshow, S., and Sturdivant, R. X. (Eds.): *Applied logistic regression*, John Wiley &
658 Sons, New Jersey, 511 pp, ISBN: 978-0-470-58247-3, 2013.
- 659 Hugenholtz, C. H., and Wolfe, S. A.: Recent stabilization of active sand dunes on the Canadian prairies and
660 relation to recent climate variations, *Geomorphology*, 68, 131–147,
661 <https://doi.org/10.1016/j.geomorph.2004.04.009>, 2005.
- 662 Instituto Nacional de Estadística y Censos (INDEC), Censo Nacional de Población, Hogares y Viviendas:
663 https://www.indec.gob.ar/ftp/cuadros/poblacion/sintesis_resultados_censo2022.pdf, last Access 6
664 May 2025.
- 665 Isla, F.I.: Holocene sea-level fluctuation in the southern hemisphere, *Quat. Sci. Rev.*, 8, 359–368.
666 [https://doi.org/10.1016/0277-3791\(89\)90036-X](https://doi.org/10.1016/0277-3791(89)90036-X), 1989.
- 667 Isla, F.I.: The flooding of the San Matías Gulf: the Northern Patagonia Sea-level curve, *Geomorphology*,
668 203, 60–65. <https://doi.org/10.1016/j.geomorph.2013.02.013>, 2013.
- 669 Isla, F.I.: Coastal barriers from Argentina: Buenos Aires, Patagonia and Tierra del Fuego, *Quat. Environ.*
670 *Geosci.*, 7, 1–9, <https://doi.org/10.5380/abequa.v8i1.43783>, 2017.
- 671 Jackson, D.W., Costas, S., González-Villanueva, R., and Cooper, A.: A global ‘greening’ of coastal dunes:
672 an integrated consequence of climate change? *Glob. Planet. Chang.*, 182, 103026
673 <https://doi.org/10.1016/j.gloplacha.2019.103026>, 2019a.
- 674 Jackson, D.W., Costas, S., and Guisado-Pintado, E.: Large-scale transgressive coastal dune behaviour in
675 Europe during the Little Ice Age, *Glob. Planet. Chang.*, 175, 82–91.
676 <https://doi.org/10.1016/j.gloplacha.2019.02.003>, 2019b.
- 677 Jansche, M.: Maximum expected F-measure training of logistic regression models. In *Proceedings of*
678 *Human Language Technology Conference and Conference on Empirical Methods in Natural*
679 *Language Processing*, Vancouver, Canada, 6–8 October 2005, 692–699, 2005.
- 680 Kalil, A. C., Mattei, J., Florescu, D. F., Sun, J., and Kalil, R.: Recommendations for the assessment and
681 reporting of multivariable logistic regression in transplantation literature, *Am. J Transplant.*, 10,
682 1695–1703, <https://doi.org/10.1111/j.1600-6143.2010.03141.x>, 2010.
- 683 Klink, K.: Climatological mean and interannual variance of United States surface wind speed, direction and
684 velocity 1, *Int. J. Climatol.*, 19, 471–488. [https://doi.org/10.1002/\(SICI\)1097-0088\(199904\)19:5<471::AID-JOC367>3.0.CO;2-X](https://doi.org/10.1002/(SICI)1097-0088(199904)19:5<471::AID-JOC367>3.0.CO;2-X), 1999.
- 686 Koerth, J., Vafeidis, A. T., Hinkel, J., and Sterr, H.: What motivates coastal households to adapt pro-actively
687 to sea-level rise and increasing flood risk? *Reg. Environ. Change*, 13, 897–909,
688 <https://doi.org/10.1007/s10113-012-0399-x>, 2013.
- 689 Kokot, R. R., and Favier-Dubois, C. M.: Evolución geomorfológica de la bahía de San Antonio, Provincia
690 de Río Negro, *Rev. Asoc. Geol. Arg.*, 74, 315–325, e-ISSN: 0004-4822, 2017.
- 691 Lancaster, N.: Development of linear dunes in the southwestern Kalahari, southern Africa, *J. Arid Environ.*,
692 14, 233–244, [https://doi.org/10.1016/S0140-1963\(18\)31070-X](https://doi.org/10.1016/S0140-1963(18)31070-X), 1988.
- 693 Lemeshow, S., and Hosmer, D. W.: A review of goodness of fit statistics for use in the development of



- 694 logistic regression models, *Am. J. Epidemiol.*, 115, 92–106,
695 <https://doi.org/10.1093/oxfordjournals.aje.a113284>, 1982.
- 696 Levin, N., Neil, D., and Syktus, J.: Spatial variability of dune form on Moreton Island, Australia, and its
697 correspondence with wind regime derived from observing stations and reanalyses, *Aeolian Res.*,
698 15, 289–300, <https://doi.org/10.1016/j.aeolia.2014.06.006>, 2014.
- 699 Lizuain, A. and Sepúlveda, E.: Geología del Gran Bajo del Gualicho (Provincia de Río Negro) 7º Congreso
700 Geológico Argentino, Neuquén, Argentina, April 1978, 407–422, 1978.
- 701 Lombardo, L., Cama, M., Conoscenti, C., Märker, M., and Rotigliano, E. J. N. H.: Binary logistic regression
702 versus stochastic gradient boosted decision trees in assessing landslide susceptibility for multiple-
703 occurring landslide events: application to the 2009 storm event in Messina (Sicily, southern Italy),
704 *Nat. Hazards*, 79, 1621–1648, <https://doi.org/10.1007/s11069-015-1915-3>, 2015.
- 705 López Alfonsín, R., Coccia, M.E., Fauqué, L.E., Castaños, C., and Olvar, N.M.: Estudio para el
706 ordenamiento territorial de la Orla Atlántica Rionegrina: Desde La Lobería a Bahía Creek, Consejo
707 Federal de Inversiones, Buenos Aires, 141 pp., 2012.
- 708 Louassa, S., Merzouk, M., and Merzouk, N. K.: Sand drift potential in western Algerian Hautes Plaines,
709 *Aeolian Res.*, 34, 27–34, <https://doi.org/10.1016/j.aeolia.2018.07.002>, 2018.
- 710 Mancini, M.V., Paez, M.M., Prieto, A.R., Stutz, S., Tonello, M., and Vilanova, I.: Mid- Holocene climatic
711 variability reconstruction from pollen records (32–52 S, Argentina), *Quat. Int.*, 132, 47–59,
712 <https://doi.org/10.1016/j.quaint.2004.07.013>, 2005.
- 713 Marcomini, S., and Maidana, N.: Response of Eolian ecosystems to minor climatic changes, *J. Coast. Res.*,
714 39, 204–208, <https://www.jstor.org/stable/25741562>, 2006.
- 715 Marcos, M.A., and Mancini, M.V.: Modern pollen and vegetation relationships in Northeastern Patagonia
716 (Golfo San Matías, Río Negro), *Rev. Palaeobot. Palynol.*, 171, 19–26,
717 <https://doi.org/10.1016/j.revpalbo.2011.11.007>, 2012.
- 718 Marcos, M.A., Espinosa, M.A., and Mancini, M.V.: Múltiples Indicadores de los cambios ambientales
719 desde el Holoceno Medio en el Noreste de Patagonia (Bajo de la Quinta), Argentina, *Ameghiniana*,
720 51, 344–360, <https://doi.org/10.5710/AMGH.28.03.2014.793>, 2014.
- 721 Michel, S., Avouac, J. P., Ayoub, F., Ewing, R. C., Vriend, N., and Heggy, E.: Comparing dune migration
722 measured from remote sensing with sand flux prediction based on weather data and model, a test
723 case in Qatar, *Earth Planet. Sci. Lett.*, 497, 12–21, <https://doi.org/10.1016/j.epsl.2018.05.037>,
724 2018.
- 725 Miot da Silva, G., and Hesp, P.A.: Increasing rainfall, decreasing winds, and historical changes in Santa
726 Catarina dunefields, Southern Brazil, *Earth Surf. Process. Landf.*, 38, 1036–1045,
727 <https://doi.org/10.1002/esp.3390>, 2013.
- 728 Miot da Silva, G., Martinho, C.T., Hesp, P.A., Keim, B.D., and Ferligo, Y.: Changes in dunefield
729 geomorphology and vegetation cover as a response to local and regional climate variations, *J.*
730 *Coast. Res.*, 65, 1307–1312, <https://doi.org/10.2112/SI65-221.1>, 2013.
- 731 Montes, A., Rodríguez, S., San Martín, C., and Allard, J.: Migración de campos de dunas en cañadones
732 costeros de Patagonia. Geomorfología e implicaciones paleoclimáticas, *Rev. Soc. Geol. España* 28,
733 65–76, ISSN 2255-1379, 2015.



- 734 Montes, A., Rodríguez, S.S., and Domínguez, C.E.: Geomorphology context and characterization of
735 dunefields developed by the southern westerlies at drying Colhué Huapi shallow lake, Patagonia
736 Argentina, *Aeolian Res.*, 2, 58–70, <https://doi.org/10.1016/j.aeolia.2017.08.001>, 2017.
- 737 National Oceanic and Atmospheric Administration (NOAA)
738 <https://www.cpc.ncep.noaa.gov/data/indices/soi>, last Access 18 May 2025.
- 739 Natural Environment Research Council–British Antarctic Survey (NERC-BAS), <http://www.nerc-bas.ac.uk/icd/gjma/sam.html>, last Access 18 May 2025.
- 741 Ohlmacher, G. C., and Davis, J. C.: Using multiple logistic regression and GIS technology to predict
742 landslide hazard in northeast Kansas, USA, *Eng. Geol.*, 69, 331–343,
743 [https://doi.org/10.1016/S0013-7952\(03\)00069-3](https://doi.org/10.1016/S0013-7952(03)00069-3), 2003.
- 744 Ozbas, B., and Greenberg, M.: Correlation between Hurricane Sandy Damage along the New Jersey Coast
745 with Land Use, Dunes and Other Local Attributes, U. S. Department of Transportation,
746 Washington D. C., File 20590-0001, 61 pp., 2013.
- 747 Pasquini, A. I., Lecomte, K. L. and Depetris, P. J.: Climate change and recent water level variability in
748 Patagonia proglacial lakes, Argentina, *Glob. Planet. Change*, 63, 290–298,
749 <https://doi.org/10.1016/j.gloplacha.2008.07.001>, 2008.
- 750 Peel, M.C., Finlayson, B.L., and McMahon, T.A.: Updated world map of the Köppen- Geiger climate
751 classification, *Hydrol. Earth Syst. Sci.*, 11, 1633–1644, [https://doi.org/10.5194/hess-11-1633-](https://doi.org/10.5194/hess-11-1633-2007)
752 [2007](https://doi.org/10.5194/hess-11-1633-2007), 2007.
- 753 Pisoni, J.P.: Los sistemas frontales y la circulación en las inmediaciones de los Golfos Norpatagónicos,
754 Ph.D. thesis, Facultad de Ciencias Exactas y Naturales, Universidad de Buenos Aires, Argentina,
755 197 pp., 2012.
- 756 Portz, L., Manzolli, R.P., Alcántara-Carrió, J., Rockett, G.C., and Barboza, E.G.: Degradation of a
757 transgressive coastal Dunefield by pines plantation and strategies for recuperation (Lagoa do Peixe
758 National Park, Southern Brazil), *Estuar. Coast. Shelf Sci.*, 259, 107483,
759 <https://doi.org/10.1016/j.ecss.2021.107483>, 2021.
- 760 Pour, S.H., Harun, S. B., and Shahid, S.: Genetic programming for the downscaling of extreme rainfall
761 events on the East Coast of Peninsular Malaysia, *Atmosphere*, 5, 914–936,
762 <https://doi.org/10.3390/atmos5040914>, 2014.
- 763 R Core Team: R: A language and environment for statistical computing, R Foundation for Statistical
764 Computing, Vienna, Austria, <https://www.R-project.org/>, 2024.
- 765 Ren, H., Gao, X., Zhao, Y., Lei, J., De Maeyer, P., and De Wulf, A.: Strong-wind events control barchan
766 dune migration, *Commun. Earth Environ.*, 5, 278, <https://doi.org/10.1038/s43247-024-01444-1>,
767 2024.
- 768 Robeson, S. M., and Shein, K. A.: Spatial coherence and decay of wind speed and power in the north-
769 central United States, *Phys. Geogr.*, 18, 479–495,
770 <https://doi.org/10.1080/02723646.1997.10642631>, 1997.
- 771 Rudgers, J. A., and Maron, J. L.: Facilitation between coastal dune shrubs: a non-nitrogen fixing shrub
772 facilitates establishment of a nitrogen-fixer, *Oikos*, 102, 75–84, ISSN 0030-1299, 2003.
- 773 Rusticucci, M., Kysely, J., Almeida, G., and Lhotka, O.: Long-term variability of heat waves in Argentina



- 774 and recurrence probability of the severe 2008 heat wave in Buenos Aires, *Theor. Appl. Climatol.*,
775 124, 679–689, <https://doi.org/10.1007/s00704-015-1445-7>, 2016.
- 776 Saavedra, M.: Caracterización climática de la circulación atmosférica en América del Sur, *Revista de*
777 *Investigación de Física*, 14, 111401761, 2011.
- 778 Sander, L., Pejrup, M., Murray, A.S., Perillo, G.M.E., Rniolo, L.A., and Fruergaard, M.: Chronology and
779 late Holocene evolution of Caleta de los Loros, NE Patagonia, Argentina, *The Holocene*, 28, 1276–
780 1287, <https://doi.org/10.1177/0959683618771477>, 2018.
- 781 Schneider, C. and Gies, D.: Effects of El Niño–southern oscillation on southernmost South America
782 precipitation at 53 S revealed from NCEP–NCAR reanalyses and weather station data, *Int. J.*
783 *Climatol.*, 24, 1057–1076, <https://doi.org/10.1002/joc.1057>, 2004.
- 784 Schober, P., Boer, C., and Schwarte, L. A.: Correlation coefficients: appropriate use and interpretation,
785 *Anesth. Analg.*, 126, 1763–1768, DOI:10.1213/ANE.0000000000002864, 2018.
- 786 Sepúlveda, E.G. (Ed.): *Hoja Geológica 38I, Gran Bajo del Gualicho*. Provincia de Río Negro, Servicio
787 Geológico Minero Argentino, Buenos Aires, Argentina, 61 pp., 1983.
- 788 Servicio de Hidrografía Naval (SHN): <http://www.hidro.gov.ar/DA/DatosAbiertos.asp>, last Access 15 May
789 2025.
- 790 Servicio Meteorológico Nacional (SMN): <https://www.smn.gov.ar/estadisticas>, last Access 18 May 2025.
- 791 Servicio Meteorológico Nacional (SMN): https://www.smn.gov.ar/como_nos_afecta, last Access 17 May
792 2025.
- 793 Snedden, G. A., and Steyer, G. D.: Predictive occurrence models for coastal wetland plant communities:
794 Delineating hydrologic response surfaces with multinomial logistic regression, *Estuar. Coast.*
795 *Shelf Sci.*, 118, 11–23, <http://dx.doi.org/10.1016/j.ecss.2012.12.002>, 2013.
- 796 Sperandei, S.: Understanding logistic regression analysis, *Biochem. Med.*, 24, 12–18,
797 <https://doi.org/10.11613/BM.2014.003>, 2014.
- 798 Steyerberg, E. W., Harrell Jr, F. E., Borsboom, G. J., Eijkemans, M. J. C., Vergouwe, Y., and Habbema, J.
799 D. F.: Internal validation of predictive models: efficiency of some procedures for logistic
800 regression analysis, *J. Clin. Epidemiol.*, 54, 774–781, [https://doi.org/10.1016/S0895-](https://doi.org/10.1016/S0895-4356(01)00341-9)
801 [4356\(01\)00341-9](https://doi.org/10.1016/S0895-4356(01)00341-9), 2001.
- 802 Stoltzfus, J. C.: Logistic regression: a brief primer, *Academic Emergency Medicine*, 18, 1099–1104,
803 <https://doi.org/10.1111/j.1553-2712.2011.01185.x>, 2011.
- 804 Thornthwaite, C. W.: An approach toward a rational classification of climate, *Geog. Rev.*, 38, 55–94,
805 <https://doi.org/10.2307/210739>, 1948.
- 806 Toffani, M.: Estudio morfodinámico de las dunas del campo eólico de Bahía Creek, Río Negro, Patagonia
807 Argentina, *Latin American Journal of Sedimentology and Basin Analysis*, 27, 55–79, ISSN 1851-
808 4979, 2020.
- 809 Toffani, M., Caselli, A.T., and Lothari Inaudi, L.D.: Estudio de los acantilados activos y del campo de
810 dunas de Bahía Creek, Río Negro, Argentina, como base para la elaboración de un mapa de peligro
811 geológico, *Rev. Asoc. Geol. Argent.*, 77, 31–46. ISSN: 0004-4822, 2020.
- 812 Toffani, M., Hesp, P., Isla, F.I., and Casadío, S.: Evolutionary stages of active to vegetated coastal
813 transgressive dune fields in the San Matías Gulf coast, Argentina, *Geomorphology* 461, 109289,



- 814 <https://doi.org/10.1016/j.geomorph.2024.109289>, 2024.
- 815 Touma, J. S.: Dependence of the wind profile power law on stability for various locations, *J. Air Pollut.*
816 *Control Assoc.*, 27, 863–866, <https://doi.org/10.1080/00022470.1977.10470503>, 1977.
- 817 Tsoar, H.: Sand dunes mobility and stability in relation to climate, *Physica A*, 357, 50–56,
818 <https://doi.org/10.1016/j.physa.2005.05.067>, 2005.
- 819 Tsoar, H., and Blumberg, D.G.: Formation of Parabolic Dunes from Barchan and Transverse Dunes along
820 Israel's Mediterranean Coast, *Earth Surf. Process. Landf.*, 27, 1147–1161,
821 <https://doi.org/10.1002/esp.417>, 2002.
- 822 del Valle, H.F., Rostagno, C.M., Coronato, F.R., Bouza, P.J., and Blanco, P.D.: Sand dune activity in North-
823 Eastern Patagonia, *J. Arid Environ.*, 72, 411–422, <https://doi.org/10.1016/j.jaridenv.2007.07.011>,
824 2008.
- 825 Vergara Dal Pont, I. P., Caselli, A. T., Moreiras, S. M., and Lauro, C.: Recent coastal geomorphological
826 evolution in the Negro River's mouth (41 S), Argentinean Patagonia, *J. Coast. Res.*, 33, 1367–
827 1375, <https://doi.org/10.2112/JCOASTRES-D-16-00060.1>, 2017.
- 828 Wang, G.: Agricultural drought in a future climate: results from 15 global climate models participating in
829 the IPCC 4th assessment, *Clim. Dyn.*, 25, 739–753, <https://doi.org/10.1007/s00382-005-0057-9>,
830 2005.
- 831 Wei, Q., and Dunbrack Jr, R. L.: The role of balanced training and testing data sets for binary classifiers in
832 bioinformatics, *PloS one*, 8, e67863, <https://doi.org/10.1371/journal.pone.0067863>. 2013.
- 833 Wörner, S., Dragani, W.C., Echevarría, E.R., Carrasco, M., and Barón, P.J.: An estimation of the possible
834 migration path of the Pacific Oyster (*Crassostrea gigas*) along the northern coast of Patagonia,
835 *Estuaries and coasts*, 42, 806–821, <https://doi.org/10.1007/s12237-018-00492-z>, 2019.
- 836 Yizhaq, H., Ashkenazy, Y., and Tsoar, H.: Why do active and Stabilized Dunes Coexist under the same
837 Climatic Conditions? *Phys. Rev. Lett.*, 98, 188001, <https://doi.org/10.1103/PhysRevLett.98.188001>, 2007.
- 839 Yizhaq, H., Ashkenazy, Y., Levin, N., and Tsoar, H.: Spatiotemporal model for the progression of
840 transgressive dunes, *Physica A*, 392, 4502–4515, <https://doi.org/10.1016/j.physa.2013.03.066>,
841 2013.
- 842 Zavala, C., and Freije, H.: Geología de los acantilados, in: *Las mesetas patagónicas que caen al mar: la*
843 *costa rionegrina*, edited by: Masera, R., Lew, J. and Serra Peirano, Gobierno de Río Negro,
844 Viedma, Argentina, 187–199, 2005.
- 845 Zhu, W.: $p < 0.05, < 0.01, < 0.001, < 0.0001, < 0.00001, < 0.000001, \text{ or } < 0.0000001, \dots$, *J. Sport Health Sci.*,
846 5, 77–79, <http://dx.doi.org/10.1016/j.jshs.2016.01.019>, 2016.